Atmospheric Research 237 (2020) 104858

Contents lists available at ScienceDirect

Atmospheric Research

journal homepage: www.elsevier.com/locate/atmosres

Analysis of the impacts of atmospheric circulation patterns on the regional air quality over the geographical center of the Eurasian continent

Gulden Ormanova[a,b,*], Ferhat Karaca[a,b,*], Nina Kononova[c]

[a] Department of Civil and Environmental Engineering, Nazarbayev University, Nur-Sultan 010000, Kazakhstan
[b] The Environment & Resource Efficiency Cluster (EREC), Nazarbayev University, Nur-Sultan 010000, Kazakhstan
[c] Institute of Geography, Laboratory of Climatology, Russian Academy of Sciences, Moscow 119017, Russia

ARTICLE INFO

Keywords:
Air pollution episode
Atmospheric circulation
Anticyclone stagnation
Atmospheric blocking
ECM types
Astana
Central Asia

ABSTRACT

There is growing scientific interest in the impact of atmospheric circulation on regional air quality; however, it is poorly studied in Central Asia. This study is the first assessment of the evidence-based relations between air pollution episodes and the elementary circulation mechanisms (ECMs, by the classification from Dzerdzeevskii et al.) with atmospheric blocking process effects on an urban atmosphere over the geographical center of the Eurasian continent. The capital city of Kazakhstan, Nur-Sultan, is selected as the study location since it is located in the north of the Kazakh Uplands in a dry steppe zone. First, an episode identification procedure using multiple stations and multiple-pollutant time series data is proposed. After the identification of the aggregated pollutant episodes during the heating and non-heating periods in 2017, their relations with blocking anticyclones and cyclones are further investigated by checking the reversal of meridional gradients in the 500 hPa and 850 hPa geopotential height (GPH) maps. In total, 12 and 9 pollution episodes lasting an average of 5 days were identified in heating and non-heating periods, respectively. Following the calendar of continuous ECM changes, the type of ECM is determined for each episode, and then, the types of ECMs with atmospheric circulation and trajectory characteristics corresponding to the episodes were analyzed in detail. The findings suggest that i) regional and local air pollution levels on the Eurasian Steppes are actively controlled by regional meteorological variations, ii) the northern streams of cold Arctic air spread to the region and Siberian anticyclone reaches in winter, leading to extreme negative air temperature anomalies that contribute to the further cooling of the Arctic air and formation of extensive stationary anticyclones with blocking effects over the region, iii) a cold season circulation type, ECM 13w, was one of the most dominant ECMs with approximately 23% annual prevalence causing 30% of all the episodes, iv) ECMs 11a, 5a, and 5b were also associated with much higher pollution levels (up to 4-fold increases over the annual average), but they had lower prevalences (up to 5%). As a result, it was demonstrated that the regional climate conditions with particular ECMs regulate the ventilation characteristics of the atmosphere over the study area, and local air pollution concentrations increase to extreme levels and remain there longer, particularly during stationary anticyclone periods.

1. Introduction

Changes in the level of air pollution in a city as a whole are determined by many factors, including anthropogenic and natural sources of pollution, atmospheric circulation patterns, the composition of the atmosphere, meteorological conditions, and meso- and microclimatic features of the urban environment (Malek et al., 2006; Zhou et al., 2018). To investigate the mechanisms of the formation of pollutants, many scientists examine *air pollution episodes*, which are dependent on the meteorological conditions of a region from synoptic and mesoscale perspectives (Gangoiti et al., 2002; Cheng et al., 2018; Molepo et al., 2019). An air pollution episode can be characterized by an unusual mixing of emissions and favorable meteorological conditions, which lead to a high level of air pollution over an urban area for up to several days.

The anatomy of an air pollution episode may be well associated with still air created by low wind speeds and temperature inversion (Sun et al., 2019; Wang et al., 2014). Therefore, many researchers have begun to study sources of air pollutants and their relationship with boundary-layer (Zhao et al., 2019) and synoptic circulation patterns (Liu et al., 2019; Toro et al., 2019; Lejenas and Holmén, 1996), continental temperature inversion characteristics (Bailey et al., 2011) and

* Corresponding authors at: Department of Civil and Environmental Engineering, Nazarbayev University, Nur-Sultan 010000, Kazakhstan.
E-mail addresses: gulden.ormanova@nu.edu.kz (G. Ormanova), ferhat.karaca@nu.edu.kz (F. Karaca).

https://doi.org/10.1016/j.atmosres.2020.104858
Received 4 September 2019; Received in revised form 23 December 2019; Accepted 15 January 2020
Available online 17 January 2020
0169-8095/

their potential sources (Hong et al., 2019; Wang et al., 2009). For example, Shin et al. (2017) and Michaelides et al. (2017) used the microphysical and optical properties of remote sensing imagery to characterize atmospheric aerosol episodes. Several other studies have examined the chemical components of aerosols during air pollution episodes (Hassan and Khoder, 2017; Chen and Xie, 2014) and have demonstrated the impact of such episodes on human health (Monteiro et al., 2018; Fenech et al., 2019).

The duration of such episodes is mainly influenced by the processes of atmospheric blocking and atmospheric stagnation, which contribute to the appearance of severe frosts in winter and heatwaves in summer (Lupo et al., 1997; Mokhov et al., 2014). Atmospheric blocking is a stable atmospheric process due to the formation of a high warm and inactive anticyclone in the middle troposphere at the mid- and high latitudes (Lee and Jhun, 2006). Any blockages in the atmosphere lead to a disturbance in the usual form of circulation and trigger a cascade of weather anomalies with different characteristics in adjacent regions (Antokhina et al., 2018). Usually, blocking anticyclones are weather-resistant systems, and their average life expectancy is five to ten days, less often about two weeks. The nonlinear instability of Rossby waves with intensive energy exchanges with both planetary waves and atmospheric vortices is a cause for the formation of such blocking anticyclones (Nascimento and Ambrizzi, 2002). The main features of the circulation processes are the evolution and movement of large-scale jet streams - cyclones and anticyclones in a particular region. In the meteorological practice of weather forecasting, the classifications of atmospheric circulations are widely used, and several studies have investigated their atmospheric blocking effects in the Northern Hemisphere (Rex, 1950a, 1950b; Barriopedro et al., 2006; Tyrlis and Hoskins, 2007; Pfahl et al., 2015). Types of atmospheric circulations are classified based on their essential characteristics of their pressure gradient.

Air pollution caused by urbanization and the Industrial Revolution has become a major problem in recent decades. As an example, Nur-Sultan, the new capital of Kazakhstan, was built only 20 years ago in the Great Steppe, and it has become one of the most polluted cities in Central Asia. Kazakhstan is located in an essential but poorly studied location in terms of meteorological and geographical impacts on air pollution (Kumar et al., 2018). The location of Kazakhstan makes it scientifically crucial in terms of atmospheric research since its remoteness from the oceans and its territory and size (it is the largest landlocked country in the world and is located on the Eurasian Steppe) and its location between two totally different climatic regions: the Middle East and Siberia (a region where the air masses of the cold north and the hot south meet).

Anticyclones over Kazakhstan are formed in two ways. These are either blocking anticyclones that move from the Arctic through Eastern Siberia to Kazakhstan and staying there for a long time or that develop onsite and permanently stay in the dry, hot air. The territory of Nur-Sultan frequently experiences anticyclone and heatwave systems since it is situated in the center of regional atmospheric circulation systems. After the dispersion of the blocking effects, accumulated pollutants in the local urban atmosphere can make even more significant and detectable contributions to the global atmospheric circulation. Consequently, the polluted air from industrial cities in Eastern Siberia impacts Kazakhstan, while polluted northern Kazakh cities affect other regions (e.g., the Mongolian territory). As a result, understanding the impacts of atmospheric circulation over the study area is essential for understanding not only local pollution episodes but also the potential impacts of long-range transportation.

This study aimed to analyze and assess the influence of atmospheric circulation on air pollution levels over the geological center of the Eurasian continent, particularly in Nur-Sultan, Kazakhstan. This study is the first assessment of the evidence-based relations between air pollution episodes and the elementary circulation mechanisms (ECMs by the classification scheme used by Dzerdzeevskii et al.) with atmospheric blocking process effects over the study region. It also suggests a novel episode identification method based on multiple stations and multiple-pollutant data.

2. Methodology

2.1. Study area

The capital city of Kazakhstan is ***Nur-Sultan*** (formerly known as Astana), which is the second coldest capital city in the world after Ulan Bator (Mongolia) and before Ottawa (Canada). It is located north of the Kazakh Uplands (Saryarka, 51° 10′ N, 71° 26′ E) in a dry steppe zone, a subzone of arid fescue-feather-grass steppes. Nur-Sultan has become one of the fastest growing and urbanizing cities over the last 20 years. The growing trends in the population, industrial enterprises, and number of automobiles are accompanied by significant changes in the natural landscapes and conditions in the city and its suburbs and result in the deterioration of the ecological qualities of the urban environment, especially air pollution. Nur-Sultan is among the most air-polluted cities in the world with elevated and long-term PM_{10} and SO_2 concentrations (Kerimray et al., 2018).

The study region is located in the zone of sharply continental climate – long, cold winters and moderately dry, hot summers. The average annual, summer, and winter temperatures are approximately 3 °C, 20 °C, and − 15 °C, respectively. There are cases with extreme summer heatwaves up to 40 °C when hot air masses of the Caspian lowland and Central Asian deserts arrive and cold frosts down to −50 °C in winter when the city receives Siberian frosts. Winter is long; it typically starts in mid-November and lasts 4–5 months with a stable snow cover. Summer is shorter and lasts slightly longer than three months with dust storms and dry winds. The location of the study area with monitoring stations used in this study and the location of power plants are given in Fig. 1.

2.2. Data collection and assessment

In this research, the hourly concentrations of air pollutants, including nitrogen dioxide (NO_2), nitrogen oxide (NO), carbon monoxide (CO), total suspended particles (TSP), and sulfur dioxide (SO_2) for 2017 from the Hydrometeorological Service of Kazakhstan (KazHydroMet) were used (Fig. 1). The KazHydroMet meteorological stations (Station #6, Station #7) are fully automatic wireless weather stations for professional monitoring and work based on the Vantage Pro 2 system, a nitrogen dioxide gas analyzer NO/NO_2 (P-310A), carbon monoxide gas analyzer CO ($K-100$), sulfur dioxide gas analyzer SO_2 (C-310A), and TSP and aerosol analyzer (Dust Track TSI -8530). There are five additional air pollution monitoring stations in the city (Fig. 1) (Kerimray et al., 2018); however, they are not reliable options for our proposed method since they do not provide continuous hourly data. As a result, we used data from only two stations (#6: NO_2, SO_2, CO, TSP, NO; #7: NO_2, SO_2, NO) for our assessments.

Meteorological data were obtained from mesoscale modeling atmospheric research centers of the National Centre for Atmospheric Research (NCAR, NCEP), climatic, and meteorological databases of the Hydrometeorological Centre and Hydrometeorological Research Institute, and the International Data Center of Russia. The atmospheric depth layer heights and 500 hPa and 850 hPa geopotential maps were computed using the Global Data Assimilation System (GDAS) and the NCAR Reanalysis datasets (https://www.ready.noaa.gov/READYcmet.php) (Trigo et al., 2004). Furthermore, the NOAA Hybrid Single-Particle Lagrangian Integrated Trajectory (HYSPLIT) numerical model was used to identify the possible backward trajectories of the air pollutants (Draxler and Hess, 1998). All of the forecast meteorological data available through READY (Real-time Environmental Applications and Display sYstem) comes directly from the NCEP and includes a wide range of scales (Rolph et al., 2017).

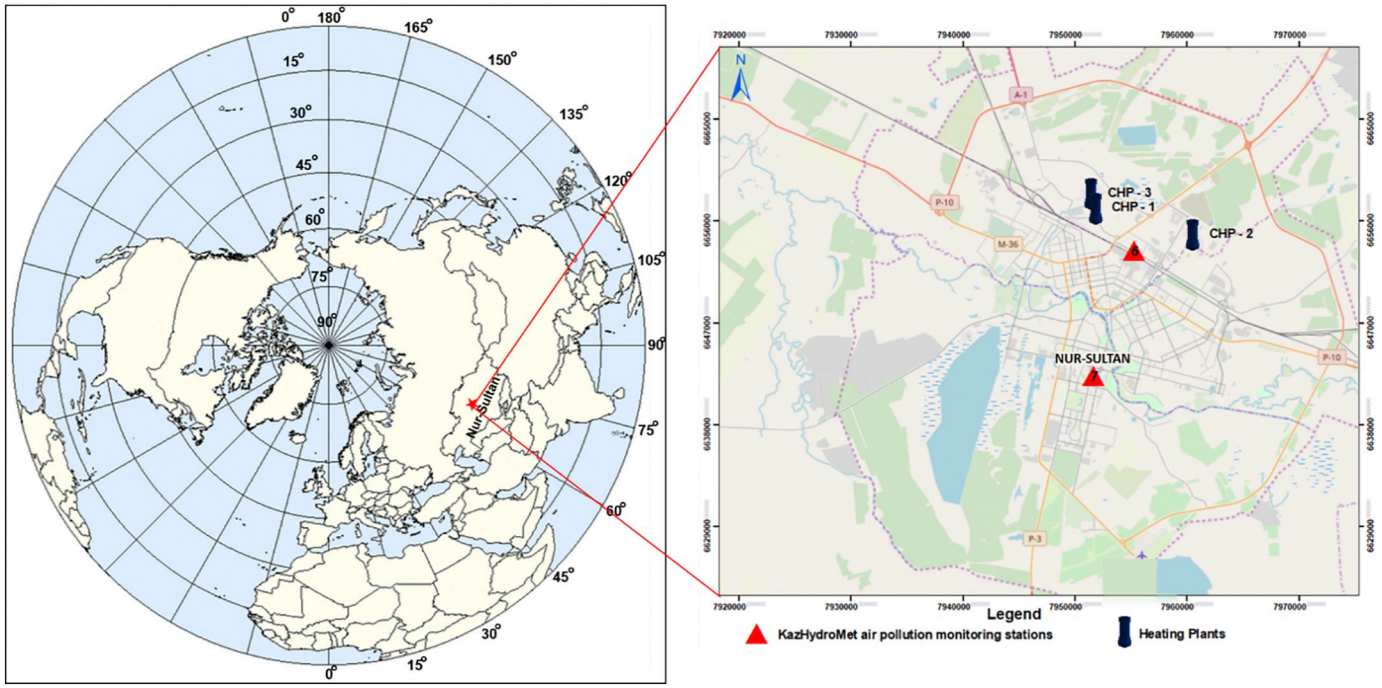

Fig. 1. The location of Nur-Sultan in the Northern Hemisphere.

2.3. Identification and classification of episode periods

In this study, air pollution episodes are identified based on a novel method involving a preselected threshold value (e.g., the top 25th percentile) of "*hourly pollution loads*." The procedure of the episode identification method follows these steps:

- All the hourly pollution data subsets (e.g., SO_2 measurements from one station) were normalized to a [0–1] scale;
- The hourly averages of the normalized pollutants (e.g., the pollutants of interest from all the available stations) were averaged and called the "*hourly pollution loads*" of the study area;
- The emission source mix and strengths were significantly different in the heating and non-heating (from mid-May until October) seasons, so the hourly pollution load data were separated into two periods;
- The threshold values of the pollution loads (the top 25th percentile) were calculated for both seasons, and all the amounts exceeding those levels were marked;
- If the sequence of the marked data was more than a day, they were identified as the pollution episode;
- Reversals of the meridional gradients in the geopotential height (GPH) maps above the boundary layer (500 hPa) with an omega-shaped high-pressure system and cyclone/anticyclone pressure systems near the boundary layer (850 hPa GPH) were also crosschecked for all the episodes if any anticyclones exist;
- Atmospheric blockings were classified as "high" or "low" according to their pressure strength and durations over the study area.

After potential episodes in 2017 were identified, they were further investigated to assess their relationship with blocking anticyclones by checking their pollution characteristics, local meteorological features, reversal of meridional gradients in the 500 hPa and 850 hPa geopotential height maps, composite maps of surface level pressure (SLP) and wind, and the ECMs of the Northern Hemisphere with atmospheric circulation and trajectory characteristics.

2.4. Classification of atmospheric circulation patterns: Elementary Circulation Mechanisms (ECMs)

The ECM types were identified using the Dzerdzeevskii et al. classification scheme. The Dzerdzeevskii classification characterizes the entire Northern Hemisphere and trajectories of cyclones and anticyclones (Dzerdzeevskii et al., 1946; Dzerdzeevskii, 1962). Their main synoptic characteristics are identified by the presence or absence of blocking processes in the Northern Hemisphere, their direction, and their quantity. In total, the ECM types were identified in 4 groups of circulations with 13 primary types and 41 subtypes (Table 1). The ECM data used in the present study are available at www.atmospheric-circulation.ru. The schematic maps of the circulation patterns and pressure systems over the Northern Hemisphere for the most prevalent ECMs (> 20% in 2017) are given in the left column along with the episode samples on the right column of Fig. 2. The coding of the ECMs includes a number and letter(s): i) the number indicates the type of

Table 1
ECM Characteristics of the atmospheric circulation groups of the Northern Hemisphere (Dzerdzeevskii et al., 1946; Dzerdzeevskii, 1962).

Circulation groups (41)	Types of ECMs *	Atmospheric pressure in the Arctic	Number of blocking processes	Number of southern cyclone outlets
Zonal (5)	1a, 1b, 2a, 2b, 2c	High	0	2–3
Zonal disturbance (13)	3, 4a, 4b, 4c, 5a, 5b, 5c, 5d, 6, 7aw, 7as,7bw, 7bs	High	1	2–3
Meridional north (21)	8a, 8bw, 8bs, 8cw, 8cs, 8dw, 8ds, 9a, 9b, 10a, 10b, 11a, 11b, 11c, 11d, 12a, 12bw, 12bs, 12cw, 12cs, 12d	High	2–4	2–4
Meridional south (2)	13w, 13 s	Low	0	3–4

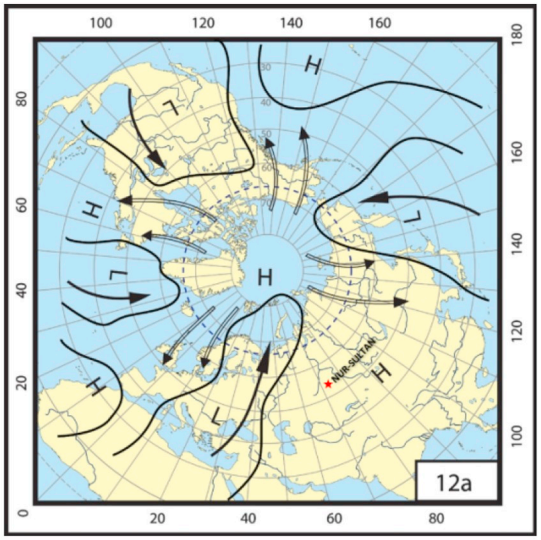

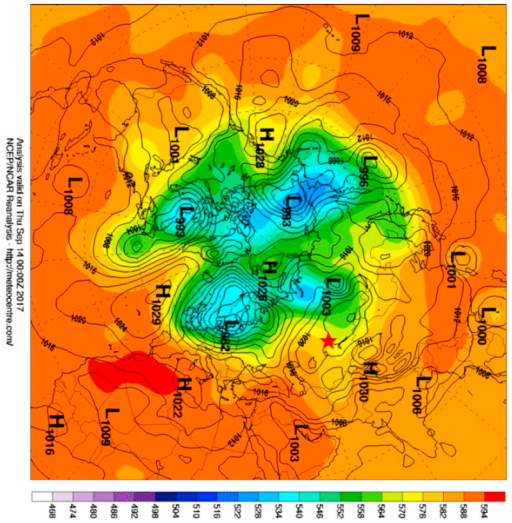

ECM 12a on 14 September 2017 (E9-S)

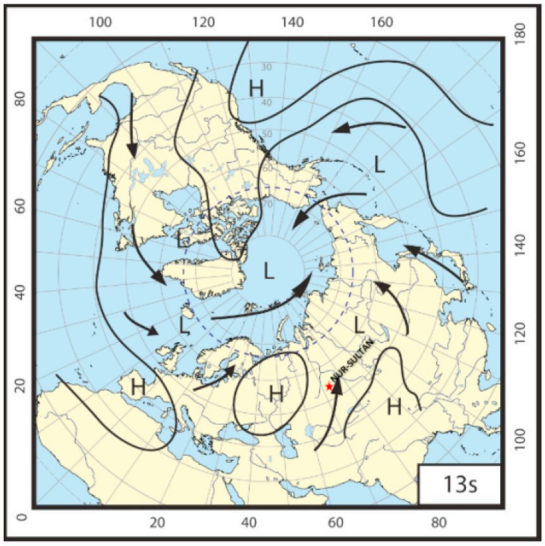

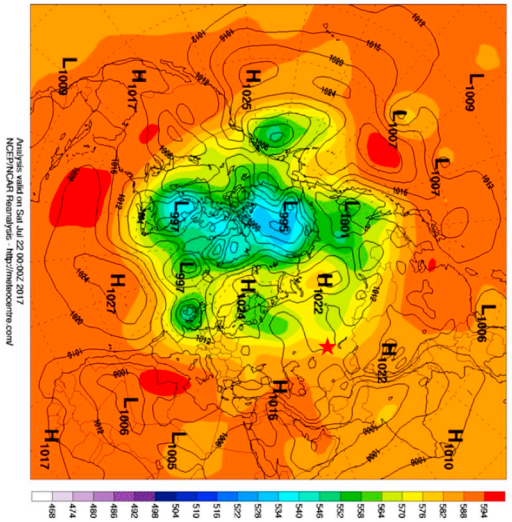

ECM 13s on 22 July 2017 (E6-S)

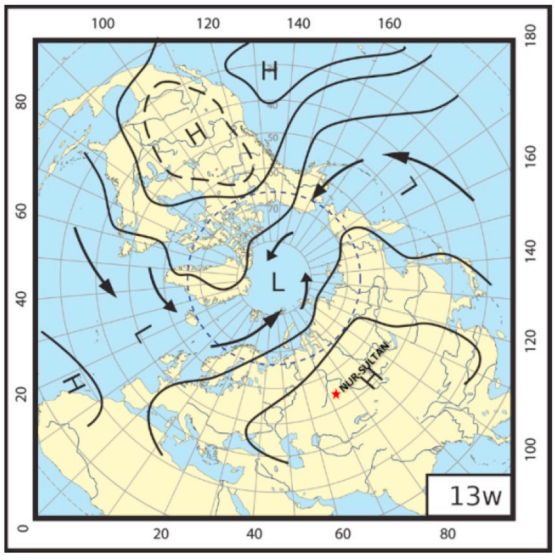

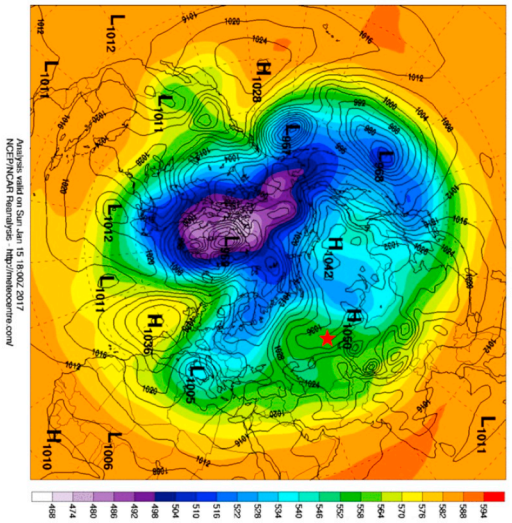

ECM 13w on 15 January 2017 (E2-W)

Fig. 2. The schematic maps of the most prevalent ECMs: 12a, 13 s, and 13w (the left-hand side column (Kononova, 2009; http://www.atmospheric-circulation.ru)) and the samples of the mean sea level pressure maps for the selected episodes (the right-hand side column) of the Northern Hemisphere in 2017, arrows: cyclone trajectories, H: high-pressure areas (with anticyclones), L: low-pressure areas (with cyclones). The location of the study are is indicated with a star.

Table 2
Descriptive statistics of the air pollution data from 2017.

		NO_2	SO_2	CO	TSP	NO
Annual	Mean (μg/m^3)	49.1	54.1	618	155	18.4
	Standard Deviation (μg/m^3)	25.5	71.3	45.4	34.9	20.8
	Kurtosis	−0.23	10.8	13.6	0.29	10.7
	Skewness	0.37	3.02	2.67	0.99	2.73
	75th percentile (μg/m^3)	65.8	57.9	764	175	23.2
	25th percentile (μg/m^3)	29.0	15.4	344	131	5.03
Non-Heating	Mean (μg/m^3)	40.8	42.5	466	137	15.2
	Standard Deviation (μg/m^3)	22.6	64.9	334	10.7	20.5
	Kurtosis	−0.02	18.9	8.20	3.56	14.7
	Skewness	0.47	3.94	2.04	1.66	3.34
	75th percentile (μg/m^3)	56.4	42.4	611	141	19.0
	25th percentile(μg/m^3)	20.2	11.6	235	129	2.8
Heating	Mean (μg/m^3)	54.9	60.9	709	161	20.5
	Standard Deviation (μg/m^3)	25.9	74.1	490	38.1	20.8
	Kurtosis	−0.31	8.2	13.1	−0.48	9.0
	Skewness	0.24	2.67	2.71	0.59	2.44
	75th percentile (μg/m^3)	73.2	71.4	858	197	27.1
	25th percentile (μg/m^3)	35.3	17.7	401	133	6.8

ECM, ii) the first letters of the alphabet (a, b, c, d) denote ECM differences within the same class in the directions of Arctic invasions or exits of southern cyclones, and iii) the letters “w” and “s” are seasonal ECM differences in the sign of the baric fields over the oceans and continents for winter and summer, respectively. However, for types 4, 9, and 10, winter ECMs are indicated by the first letters of the alphabet (4a, 9b, and 10a). Readers are directed to the extant literature for more details (Kononova, 2009, 2010; Brenčič et al., 2015). The main characteristics of all available ECMs over the study area during the study period are provided in the Supplementary Material.

3. Results and discussion

3.1. Pollution profile of the study area

The descriptive statistics of the pollution measurements are given for the yearly, non-heating, and heating periods in Table 2. When the 24-hour mean of the SO_2 concentration and the one-hour mean of the NO_2 concentration were compared with the WHO air quality health risk limits of 20 μg/m^3 and 200 μg/m^3, the matching percentiles were found to be the 32nd and 17th percentiles, respectively. Noting that most of the concentrations were significantly higher during winter, the matching percentiles increased to the 36th and 25th percentiles, respectively, during the non-heating season -albeit they improved from the heating season- they were still not close at the required level (e.g., < 35 days per calendar year, the 90th percentile) even in the summer. Pollutants have seasonality, particularly TSP, and episodes were observed more often in the heating period. Emission types and source mix create the main air quality differences between the heating and non-heating seasons, as the level of pollution increases during the heating period. The highest seasonal differences in the non-heating and heating season averages (ratio in %) are observed for the TSP values (58%), followed by the CO (35%), SO_2 (32%), NO_2 (16%), and NO (14%) values. A correlation analysis between the hourly pollutant data showed that the NO_2 and NO (R = 0.63, p < < 0.01), NO_2 and CO (R = 0.67, p < < 0.01), NO and CO (R = 0.71, p < < 0.01) pairs are significantly correlated. The TSP concentration is also correlated with the SO_2 (R = 0.33, p < .01), NO_2 (R = 0.51, p < < 0.01), and CO (R = 0.54, p < .01) values. These correlation results indicate that the correlated parameters may common sources.

The research on the air quality assessment of the cities and countries in Central Asia is limited (Rupakheti et al., 2019); however, a brief comparison was carried out for the pollution levels between Nur-Sultan and surrounding cities and countries. The annual average pollutant levels are summarized in Table 3. Typically, the region suffers from air pollution problems and Nur-Sultan is not an exception. The most polluted and populated cities are located on the eastern side of the region, for example, the Chinese cities, e.g., Beijing and Shanghai; however, Beijing has recently experienced significant pollution reductions due to the recent air pollution act and regulations (Vu et al., 2019). Moscow is also a megacity located on the northern side of the region and its pollution levels are considerably lower than Nur-Sultan. Ulaanbaatar and Bishkek are other Central Asian cities with almost at the same population and pollution levels as Nur-Sultan; however a significantly lower SO_2 level was reported in Bishkek between 2010 and 2013. To the knowledge of the authors, no reliable data are available for the other major cities in the region, e.g., Dushanbe, Ashgabat, and Tashkent.

Identification of the potential sources is beyond the scope of this paper; however, their variation and characteristics are briefly discussed to provide background knowledge for readers. The primary anthropogenic sources are coal-fired power plants (CHP-1, CHP-2, and CHP-3), located on the outskirts of the urban area (Fig. 1). The CHPs operate on full power during the harsh winter times to fulfill energy and district heating requirements. In the summer, their emission strengths are reduced since there are no heating requirements. In addition to the power plants, private district boilers produce hot water for surrounding districts. Nevertheless, a large number of houses are heated by residential boilers and heating systems with low chimneys, which make a significant contribution to the formation of a smog cover frequently observed over the right bank of the city. Mobile sources, especially around road congestion, contribute to NO_2, CO, and PM pollution levels in the inner urban structure. Registered motor vehicles use gas cylinders (83%), followed by gasoline (16%) and diesel fuels. Fugitive and uncontrolled sources of emissions from industrial activities should also be listed in the anthropogenic emission inventor. The most significant industrial activities include construction activities, metalworking, asphalt/concrete plants, light industry enterprises (tanneries and garment factories), sawmills, and brick factories.

3.2. Relations between local meteorological parameters and ground-level pollutants

Apart from the emission source characteristics and seasonal variations, the elevated hourly and daily pollution levels in seasons are mostly related to independent settings, including climate and terrain characteristics. Nur-Sultan does not experience significant microclimate variations from the entire region, and the emissions characteristics and volumes follow an almost regular daily pattern, except traffic. The city is located on the Eurasian Steppes (no hills, sea, and other significant terrain impacts), so the primary independent mechanisms on the observed episodes can be attributed to meteorological variations. Typically, a smog layer is formed in the presence of emissions under stable atmospheric conditions, and the urban area frequently experiences higher pollution levels when it is located downwind (e.g., the NW) from the CHPs.

Atmospheric stability data interpolated to the location of interest and local meteorological factors were used to assess their relationship with the pollution levels. Their correlations are presented in Table 4, and the time series of the pollutants are provided in Fig. 3. In terms of the hourly data correlations, the TSP and CO pairs are the parameters most correlated with temperature (p < < 0.001), while NO and SO_2 are the least correlated parameters. Pressure and relative humidity (RH) are always positively correlated, while temperature and the atmospheric boundary layer depth are negatively correlated with the pollutants. These results support the importance of climate parameters, including atmospheric stability and meteorological factors, on pollution levels.

3.3. Relations between ECMs and pollution levels of the region

The Dzerdzeevskii classifications of ECMs were identified for all the

Table 3
The pollution levels of Nur-Sultan and their comparison with the surrounding cities and countries, based on the annual mean concentrations of SO_2, NO_2, NO, CO, and particle masses (TSP, PM_{10}, and $PM_{2.5}$). All the units are in $\mu g/m^3$.

City/study date	Population in millions	NO_2	SO_2	CO	TSP (PM_{10})	$PM_{2.5}$	NO	References
Nur-Sultan /2017	1.1	49.1 ± 25.5	54.1 ± 71.3	618 ± 45.4	155 ± 34.9		18.4 ± 20.8	Current study
Nur-Sultan /2018	1.0	95	30	530	20	20	20	KazHydroMet (2018)
Almaty /2018	1.8	59	46	773	31	15	24	KazHydroMet (2018)
Beijing /2005	12.4	122	90	–	377	–		Gurjar et al. (2008)
Beijing /2017	19.2	45	8	900	89	58	–	Vu et al. (2019)
Shangnai /2005	18.6	73	53	–	246	–	–	Gurjar et al. (2008)
Moscow /2002–2008 period	12.1	40.2	4.4	–	32	–	–	Elansky (2014)
Ulaanbaatar /2009–2010	1.1	–	50.5	–	165	75.1	–	Amarsaikhan et al. (2014)
Bishkek /2010–2013	0.87	50–60	2–6	–	–	–	80–120	Nishanbaeva (2015)

days in 2017 and are summarized in Table 5. The most dominant ECMs were 12a (24.7%), 13w (22.7%), and 13 s (24.4%). Each of the other circulation types made up < 10% in 2017; however, three particular ECMs (11a, 5a, and 5b) are noteworthy due to the extremely high pollution levels experienced during their appearance.

Examples of the composite synoptic weather maps of the mean sea-level pressure with wind directions for selected episodes with the major ECM types (e.g., ECMs 12a, 13w, and 13 s) over the Northern Hemisphere in 2017 are provided in Fig. 4. In accordance with the position of the cyclones and anticyclones in these maps, the wind blows from high-pressure areas to low, but not in a straight line. Winds blow counterclockwise in a cyclone, to the south in the front of a cyclone and to the north behind a cyclone. In an anticyclone, the wind directions are in the opposite direction, e.g., the winds blow to the clockwise direction.

The 12a ECM was observed in almost one-fourth of the days in 2017 (e.g., Fig. 4a). This type of ECM mostly appeared during the transition period from the cold half-year to the warm one, when the Arctic anticyclone reached its most significant strength, which occurred in the southern latitudes where the underlying surface was already sufficiently heated. It occurred year-round with a maximum frequency at the beginning of May. The average pollution level under this circulation pattern was close to the annual averages (104%), which can be attributed to low anticyclones.

The 13s ECM is the second most prevalent circulation type observed (e.g., Fig. 4b). It mostly occurred from March to September and rarely in October and November. Fig. 4b represents the episode on July 22, 2017, and shows a weak low-pressure system over the region. The highest frequency was recorded in July. In terms of the local air pollution, this system was favorable with its high prevalence and slightly lower average pollution level among the other non-heating-period ECMs (e.g., 10b, 12bs, 8ds, and 9a).

The 13w ECM is the third most dominant ECM observed in 2017 (e.g., Fig. 4c). It is a heating period circulation type and is prevalent from September to May. The example given in Fig. 4c shows how a strong forcing high-pressure system forms (in the shape of an omega) over the region. The highest frequency was observed in the middle of December. The average level of the observed atmospheric pollution during this circulation mechanism was significantly higher than the annual averages (126% ± 125%). The 13w ECM created a low-level atmospheric boundary level with an average of approximately 446 m and high ground-level pressure in the study area. These results indicate that there is a clear association with cold season episodic pollution levels with this particular ECM type over the study area. The details on the episode are discussed in the next section.

Other significant pollution levels were observed in the low-prevalence ECMs of 11a (2.5%), 5a (0.6%), and 5b (0.8%) with Siberian anticyclone formation. The 11a ECM was present from early September to the first week of May. The maximum frequency fell in the first week of February during the period from November to the first week of March. The record-breaking ECM for the local pollution levels was the ECM type 5a with extreme pollution deviations from the annual averages (157% ± 164%); however, it was experienced for < 1% of 2017. During this ECM, there is one northern blocking process over Eastern Siberia. The maximum frequency occurred in December.

To investigate the main patterns in the air trajectories, 24-hour backward trajectories were calculated for each hour during certain ECM types and then clustered using the method suggested in an earlier study using HYSPLIT (Anil et al., 2017). The total spatial variance (TSV) analysis indicated that a 5-cluster solution can reasonably explain the variance in the trajectories for the dominant ECMs; however, no clustering procedure was applied for the minor ECMs due to the limited number of episodic events. The mean clusters for the five-cluster solutions for the most dominant ECM types (12a, 13w, and 13 s) are given in Fig. 5.

In general, the trajectory clusters move in a counterclockwise direction, indicating the impact of an anticyclonic force. The shortest trajectories are the slowest and lowest trajectories that travel at lower altitudes not far from the ground level (< 500 m), indicating some particular large-scale, high-pressure system blocking (e.g., Siberian Arctic). They are also associated with the highest concentrations in the episodic observations. This type of trajectory represents the most

Table 4
Pearson correlation table of the independent factors and pollutants.

		Boundary layer depth	Vertical mixing coefficient times	Friction velocity	Horizontal mixing coefficient	Temp.	RH	Wind Speed	Pressure
NO_2	R value	−0.28**	−0.34**	−0.37**	−0.32**	−0.23**	0.09**	−0.30**	0.27**
	p value	0.000	0.000	0.000	0.000	0.000	0.000	0.000	0.000
SO_2	R value	0.02	0.09**	0.09**	0.17**	−0.21**	0.06**	0.09**	0.13**
	p value	0.256	0.000	0.000	0.000	0.000	0.001	0.000	0.000
CO	R value	−0.20**	−0.26**	−0.33**	−0.26**	−0.30**	0.14**	−0.25**	0.29**
	p value	0.000	0.000	0.000	0.000	0.000	0.000	0.000	0.000
TSP	R value	−0.25**	−0.16**	−0.13**	−0.04	−0.46**	0.21**	−0.10**	0.23**
	p value	0.000	0.000	0.000	0.076	0.000	0.000	0.000	0.000
NO	R value	−0.14**	−0.19**	−0.24**	−0.21**	−0.14**	0.10**	−0.19**	0.20**
	p value	0.000	0.000	0.000	0.000	0.000	0.000	0.000	0.000

** Correlation is significant at the 0.01 level (2-tailed).

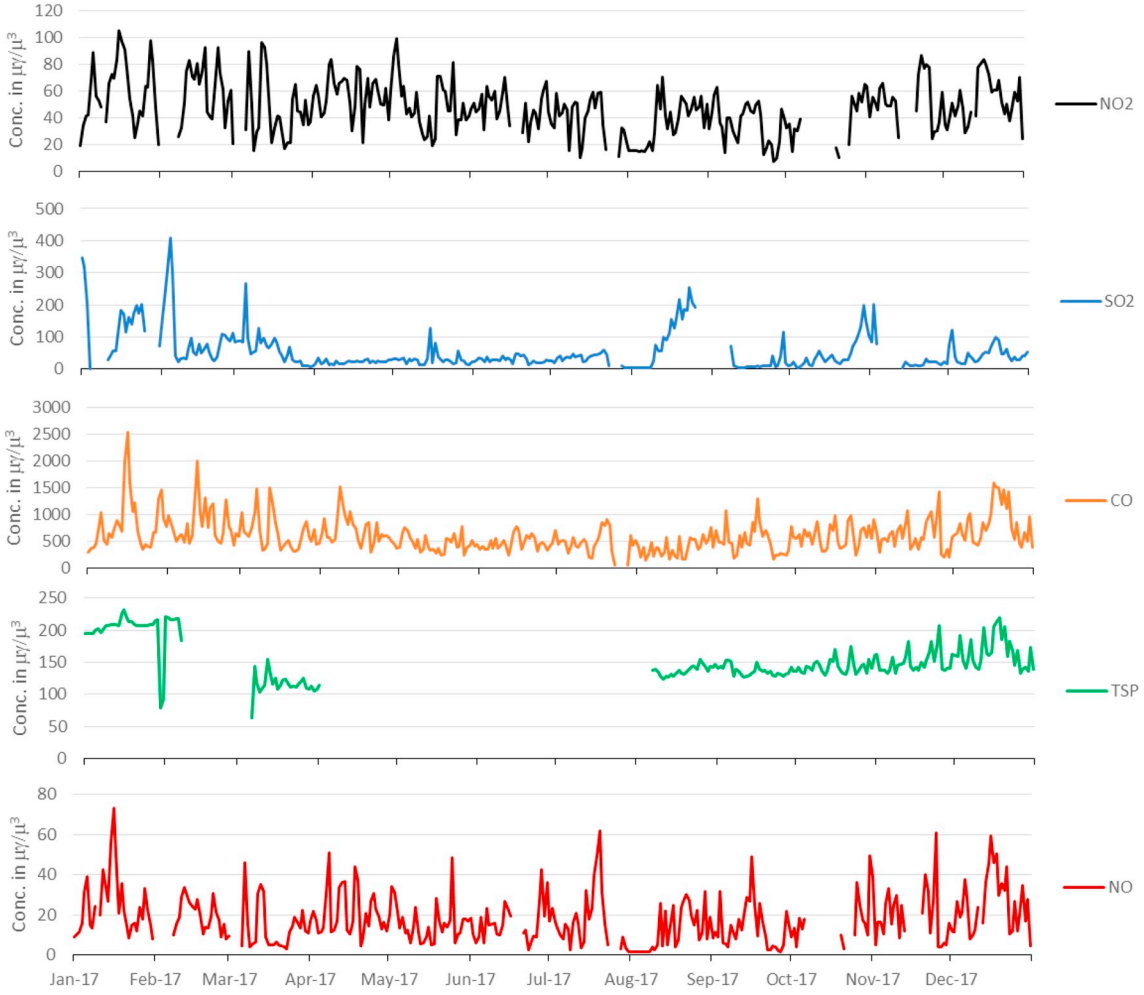

Fig. 3. Time series of observed daily averaged pollution data (station #6) in Nur-Sultan.

Table 5
Summary of the prevalence of the Dzerdzeevskii classification types of ECMs and local meteorology and pollution data in the study area (2017). * "NA" means not available.

ECM	Frequency in 2017 (%)	Contribution to the episodes (%)*	Boundary layer depth (m)	Surface Pressure (hPa)	Wind Speed (m/s)	Temp. (°C)	Average pollution deviation (± SD) from the overall annual average pollution (%)
12a	24.7%	23.1%	488	1023	2.3	2.6	104% ± 106%
13 s	24.4%	9.9%	800	1014	1.9	18.7	73% ± 72%
13w	22.7%	29.7%	446	1029	2.4	−9.6	126% ± 125%
9a	5.8%	6.6%	776	1013	2.7	16.8	84% ± 85%
12bw	2.7%	4.4%	215	1026	2.0	−4.7	116% ± 121%
11a	2.5%	5.4%	148	1035	1.3	−5.2	147% ± 150%
12bs	2.2%	2.2%	855	1013	2.7	13.7	82% ± 91%
10b	1.9%	4.4%	847	1007	2.4	19.9	104% ± 108%
3_	1.6%	4.4%	899	1011	1.9	22.7	77% ± 81%
8dw	1.6%	1.1%	120	1033	1.3	−3.6	100% ± 108%
11d	1.4%	NA	632	1019	2.6	−2.7	80% ± 84%
9b	1.4%	3.3%	693	1013	3.4	−1.8	114% ± 88%
12d	1.1%	1.1.%	593	1028	3.2	1.9	95% ± 95%
8ds	1.1%	1.1%	688	1013	1.6	15.6	73% ± 73%
2a	0.8%	NA	772	1006	1.2	25.9	93% ± 103%
5b	0.8%	NA	323	1015	1.1	9.0	133% ± 126%
8a	0.8%	2.2%	490	1026	2.9	−2.8	78% ± 87%
5a	0.6%	1.1%	113	1039	1.8	−11.4	157% ± 164%
4b	0.5%	NA	868	1007	3.1	14.4	60% ± 43%
10a	0.3%	NA	703	1025	3.5	2.1	75% ± 69%
12cs	0.3%	NA	371	1029	1.6	0.8	107% ± 103%
4c	0.3%	NA	638	1015	2.9	10.1	51% ± 39%
5d	0.3%	NA	815	1013	1.1	25.3	86% ± 79%
6_	0.3%	NA	1000	1008	3.5	20.9	61% ± 59%
2017		24.9%	618	1021	2.2	5.3	

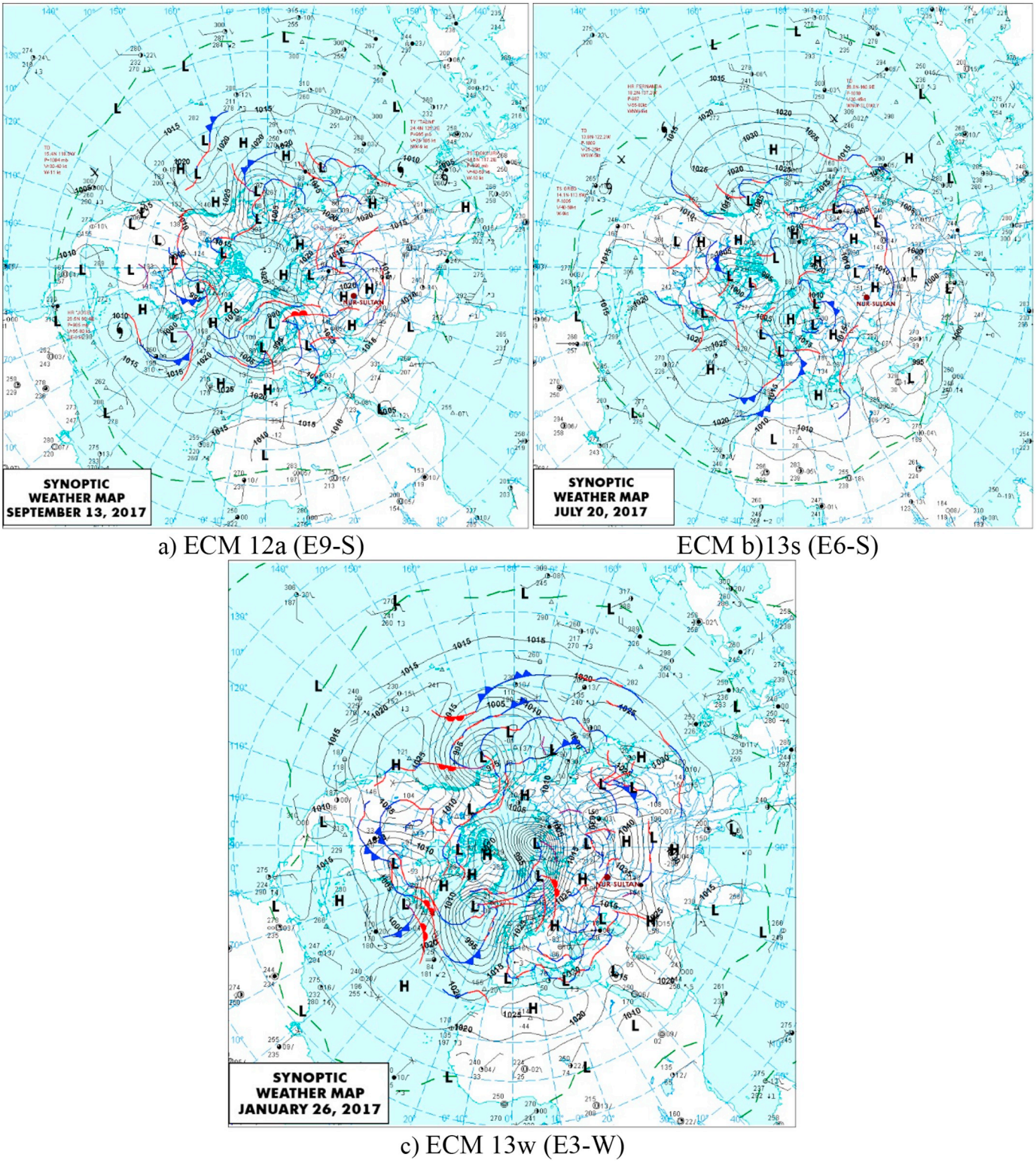

a) ECM 12a (E9-S) ECM b)13s (E6-S)

c) ECM 13w (E3-W)

Fig. 4. Examples of the composite wind direction and pressure maps for selected episodes with the major ECM types over the Northern Hemisphere in 2017 (a) ECM 12a on the 13 September 2017, E9-S; b) ECM 13 s on the 20 July 2017, E6-S; and c) ECM 13w on the 26 January 2017, E3-W; H – High-pressure areas (with anticyclones), L- low-pressure areas (with cyclones).

frequent air movements, which can be attributed to local-level pollution accumulations (Anil et al., 2017). When the trajectory clusters of the given ECM are compared, it can be seen that the dominant part (63%) of the trajectories in clusters 2 (15%), 3 (32%), and 4 (16%) of ECM 13w has such behavior. This result also supports our earlier discussions on the higher-level episodic contributions of ECM 13w. ECM 13 s is the lowest-contributing episode type among the dominant ECMs. It has the most frequent trajectory, which are fast, long, and travel a high altitude (clusters 1, 2, and 5, contributing to a total of 45% of all the ECM 13s clusters). All trajectories of the 13w episodes are travel at the lowest altitude (< 500 m), which is typically lower than the atmospheric boundary level and indicates the downward pressing force of the air

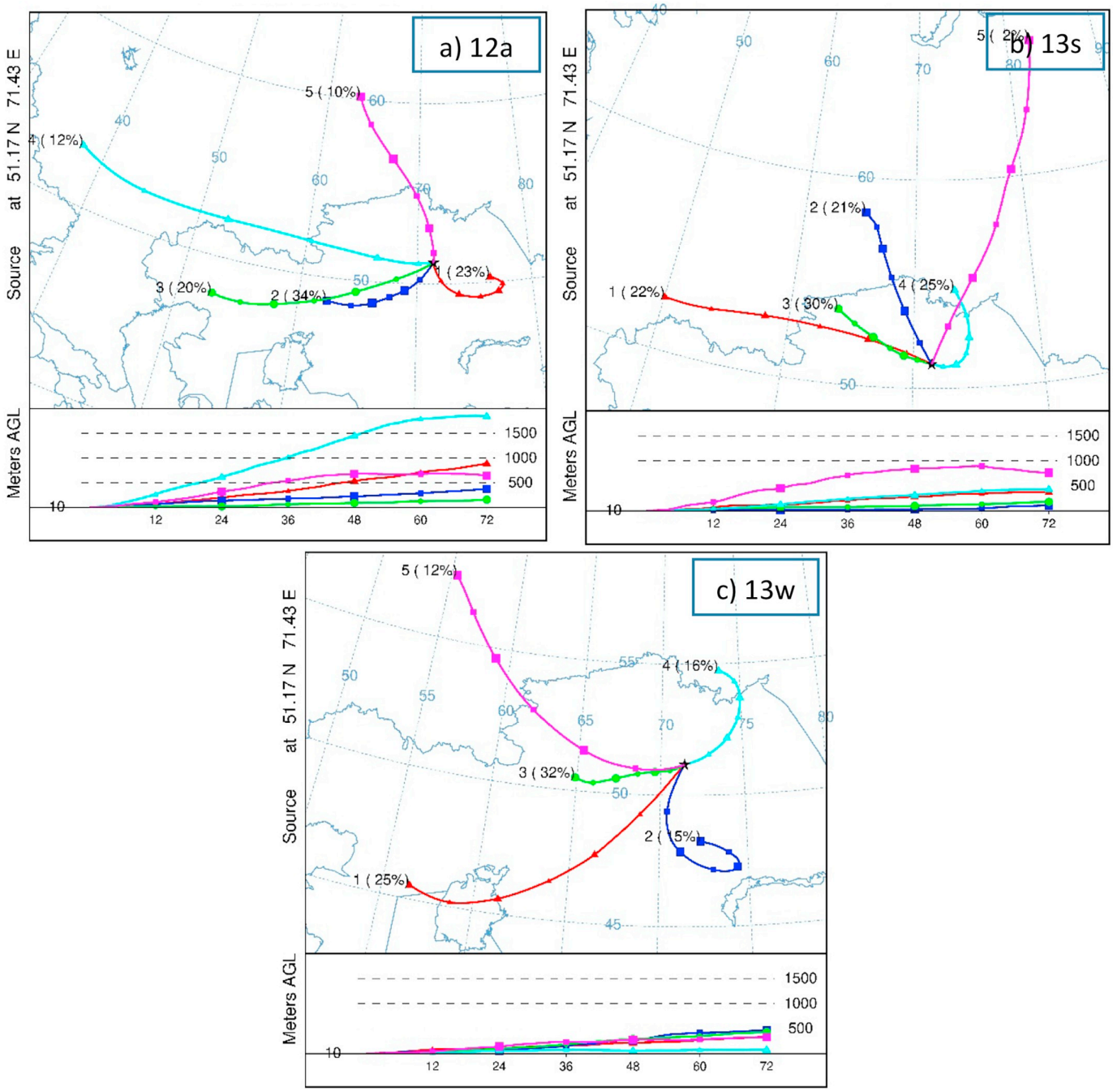

Fig. 5. The mean clusters for the five-cluster solutions for the most dominant ECM types (a) 12a, b) 13s and c) 13w).

masses over the region during the anticyclone pressure system.

3.4. Pollution episodes and their ECM characteristics

There are 12 and 9 pollution episodes in heating and non-heating periods, respectively, in 2017. The time series of the calculated pollution loads along with the threshold values of the episodes are shown in Fig. 6. The details of the identified episodes are summarized in Table 6. They typically range from 2 days to 8 days, and the longest episode is 11 days (E8-W).

All of these episode days were investigated for atmospheric blockings by the reversal of 850 hPa and 500 hPa omega (Ω)-shaped geopotential height meridional gradients having centers in the study area (6th column in Table 6). These omega blocks are a combination of two cutoff lows with one blocking high-pressure system squeezed between them. As an example, 500 hPa and 850 hPa maps are given in Fig. 7 for the E2-W episode before (10 Jan 2017), during (13 Jan 2017), and after (20 Jan 2017) its formation. All the episodes, except E5-S, were matched with the 500 hPa anticyclone blockings, but they might have some lags that do not match with the exact beginnings and endings of the episodes. Typically, an anticyclone appears first, then the pollution level starts to rise with several hours lags (up to a few days), and finally, when the blocking effect starts to lose its strength, the level of pollution decreases with local dispersion. However, numerous early-starting (e.g., E7-W, E8-W) and late-ending (e.g., E1-W, E8-W) episodes were also identified. The Siberian anticyclone does not rise to a height of > 1.5–3 km (850–700 hPa), which is also visible on the GPH maps; the pressure is already equalized above this height, and the western zonal transport was dominated by a forming, non-impeding anticyclone (Fig. 7).

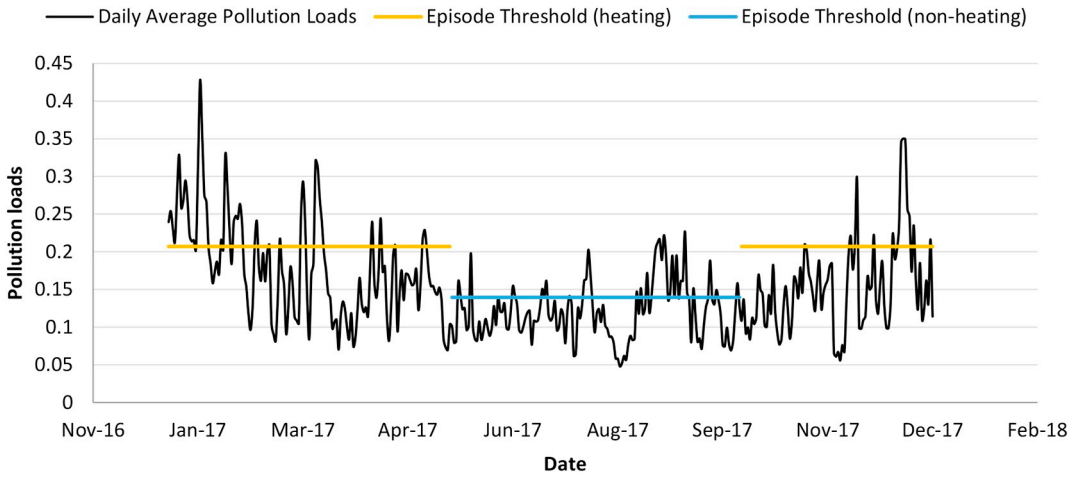

Fig. 6. The time series of the calculated pollution loads and the thresholds for the heating and non-heating season episodes.

The January, March, and December episodes are the episodes associated with the highest wintertime pressure systems over the region. During these events, the atmospheric pressure was in the range of 1020–1035 hPa over Kazakhstan, and six of the episodes (E1-W, E2-W, E3-W, E4-W, E6-W, E7-W, E11-W, and E12-W) lasting a total of 38 days were experienced. These episodes, which make up > 10% of a year, are associated with the highest level of local pollution loads. Before these episodes, southern cyclone outlets were formed in the east of the Mediterranean and passed through Kazakhstan. Arctic air was spread as an Arctic invasion leading to air cooling with clear skies over the region and pushing downward air flows in the anticyclone, which press pollutants to the surface of the earth. Then, the circulation system turned into ECM 13w, which forms in the continental air without an additional inflow of air masses from the east through Eastern Siberia. Therefore, the concentration of the pollutants increased dramatically and remained for several days. These episodes are the most recognizable on the 500 hPa maps, with the formation of an omega-shaped blocking effect.

According to the synoptic charts, three winter events, E5-W, E9-W, and E10-W, occurred in ECM 12a, an Arctic invasion through Eastern Siberia type circulation where the Mediterranean cyclone over southern European Russia was powerful and spread its fronts to Kazakhstan, although the pressure was 1015–1020 hPa.

October is the start of the heating season since the temperature falls below 10 °C. No episode was identified based on the criteria applied in this month. The atmospheric circulation and regional meteorological conditions were more appropriate for long-term transportation and did not cause local accumulation of the pollutants. At the end of October, the fronts of the Mediterranean cyclone (13w) crossed the study area followed by a wave cyclone (12a), and then the pressure dropped to 1000 hPa, causing high-level precipitation that further cleaned the local air.

The longest episode, which lasted 11 days (E8-W), was observed in April at the end of the heating season. It began with a stationary anticyclone (ECMs 13w and 8a), and then anticyclone stagnation stayed over the region. This anticyclone system led to the formation of cold weather in most parts of the country. No precipitation, and quiet and calm air conditions were observed, leading to the accumulation of pollutants with a thick smog cover over the city.

Summer episodes are not as high as the winter ones due to the strength of the emission sources, and they tended to disperse faster than winter ones by the effect of cyclonic regions with low-pressure systems (1005 hPa). This phenomenon leads to a low level of pollution in Nur-Sultan with the typical summertime ventilation systems blowing from the west when the front of the occlusion approaches. In such cyclone systems, warm air rises, and then the cold front catches up with the warm front and merges with it.

Three summer episodes (E2-S, E3-S, and E9-S) were formed under the 12a ECM type. The fronts of the Mediterranean cyclones, which enter European Russia, extended over Kazakhstan. Then, the study region was in the zone of a reduced-pressure system (1010 hPa), so the level of the E2-S episode was not as high as that of the other 12a systems. ECM 13 s was associated with the other summer episodes by the restructuring of the tropospheric flows that occurred from the meridional to the latitudinal direction, and air masses from the Atlantic began to flow to Kazakhstan. Nur-Sultan is located at the base of the Azores anticyclone. It moves westward and has a stronger influence in summer, and it reaches the study region through Moscow.

The map-based inspection of the geopotential maps provides useful information about the impacts of pressure systems over the study area. However, to make a quantitative assessment of the effects of the SLP and regional geopotential heights (850 hPa and 500 hPa) on the local pollution loads, regression analyses were performed. The SLP averages, geopotential heights for the 850 hPa, and 500 hPa geopotential maps of the episodes along with the average (local) pollution loads on the study area are provided in Fig. 8. This figure shows that the pollution loads in the air correlated well with the SLP ($R = 0.62$; $p < .01$ and $R = 0.45$; $p < .05$) and a geopotential height of 850 hPa ($R = 0.56$; $p < .01$ and $R = 0.45$; $p < .05$) during the non-heating period and heating periods. The geopotential height for the 500 hPa regression graph does not show significant correlations with the pollution loads. The SLP of the air affects the buildup of local pollution levels. During high-pressure systems, the local air becomes more stable, intensifying the pollution level buildup. The results confirm that the higher the pressure system is, the higher the pollution load ending with more extended time episodes with the formation of persistent pools of cold air over the study area. As synoptic-scale high-pressure forms over the study region, along with warm advection above the steppes, the stability of the atmosphere intensifies.

4. Conclusions

In this study, the influences of atmospheric circulation on air pollution levels over the geological center of the Eurasian continent were assessed. Elementary Circulation Mechanisms (ECMs) by the Dzerdzeevskii et al. classification were identified for each day during a one-year period (2017), and the effects of their atmospheric blocking processes over the study region were further investigated. A relationship diagram to summarize the overall relationship between ECMs and their associated pressure systems and pollution levels is illustrated in Fig. 9. Most of the ECMs with low-pressure systems in the study region resulted in low pollution levels, while high-pressure systems were

Table 6
Summary of the identified episodes (n = 12 in winter, 9 in summer) with Elementary Circulation Mechanism (ECM) classifications and their anticyclone strength of the reversal of meridional gradients in the 500 hPa and 850 geopotential height maps for 2017.

Episode names W: winter S: summer	Local pollution episode periods (duration)	Surface pressure hPa	850 hPa geopotential height	Matching anticyclone blocking periods identified by 500 hPa geopotential maps	500 hPa geopotential height	Sub-dates (ECM type)
E1 - W	02–09 Jan (8)	1015–1025–1015 (normal high - normal)	140–155 (low – high)	01–03 Jan (3)	544, (low)	01–03 (9b), 04–09 (13w)
E2 - W	13–19 Jan (7)	1025–1030 (high)	150 (normal)	12–19 Jan (8)	552, (low)	12–13 (12a), 14–19 (13w)
E3 - W	26–29 Jan (4)	1020–1025 (high)	143–145 (low)	26–31 Jan (6)	544, (low)	26–29 (13w), 30 (12a), 31 (13w)
E4 - W	12–15 Feb (4)	1030–1035 (high)	145–150 (low - normal)	11–17 Feb (7)	536, (low)	11–17 (13w)
E5 - W	23–24 Feb (2)	1015–1020 (normal – high)	140–145 (low)	21–28 Feb (8)	544, Low	21–25 (12a), 26–27 (12d), 28 (12a)
E6 - W	06–07 Mar (2)	1025–1030 (high)	155 (high)	02–08 Mar (8)	568, High	2 (13w), 3–4 (12a), 5–8 (13w)
E7 - W	12–15 Mar (4)	1025–1030 (high)	150 (normal)	14–25 Mar (12)	554, High	14–25 (13w)
E8-W	03–13 Apr (11)	1020–1025 (high)	140–155 (low – high)	06–10 Apr (5)	564, High	6 (8a), 7 (12bw), 8 (8dw), 9–11 (12a), 12–13 (9a)
E1-S	22–27 Apr (6)	1015–1025 (normal – high)	140–160 (normal – high)	17–27 Apr (11)	564, High	17–21 (12a), 22 (12bs), 23–26 (12a), 27 (13 s)
E2-S	02–07 May (6)	1010–1015 (low - normal)	145–160 (low – high)	01–05 May (5)	572, High	01–05 (12a)
E3-S	25–26 May (2)	1010–1015 (low - normal)	150 (normal)	25–27 May (2)	552, High	25 (12bs), 26 (3), 27 (9a)
E4-S	16–17 Jun (2)	1005–1010 (low)	145 (low)	14–19 Jun (6)	572, High	14–15 (2a), 16 (3), 17–19 (13 s)
E5-S	29–30 Jun (2)	1005–1010 (low)	150 (normal)	na	580, High	29–30 (3)
E6-S	18–21 Jul (4)	1010–1015 (low – normal)	150 (normal)	19–26 Jul (7)	584, High	19 (10b), 20–26 (13 s)
E7-S	20–26 Aug (7)	1015–1020 (normal – high)	150–155 (normal – high)	14–28 Aug (15)	580, High	14–23 (13 s), 24–25 (9a), 26 (12d), 27 (5d), 28 (13 s)
E8-S	03–05 Sept (3)	1010 (low)	155–150 (high – normal)	01–05 Sept (5)	584, High	01–03 (13 s), 04–05 (10b)
E9-S	13–15 Sept (3)	1015–1020 (normal – high)	155 (high)	13–15 Sept (3)	584, High	13–15 (12a)
E9-W	01–02 Nov (2)	1015–1020 (normal - high	145–150 (low – normal)	26 Oct - 02 Nov (7)	556, High	26–28 (13w), 29–02 (12a)
E10-W	21–23 Nov (3)	1010–1015 (low – normal)	140–145 (low)	20–30 Nov (11)	560, High	20–21 (12a), 22 (8dw), 23–25 (12a), 26 (12bw), 27–30 (8dw)
E11-W	14–22 Dec (9)	1015–1035 (normal - high	155 (high)	13–23 Dec (11)	560, High	13–14 (12a), 15 (12bw), 16–17 (11a), 18 (5a), 19 (12bw), 20 (11a), 21 (13w), 22–23 (12bw)
E12-W	30–31 Dec (2)	1020–1025 (high)	150 (normal)	29–31 Dec (3)	564, High	29 (13w), 30–31 (11a)

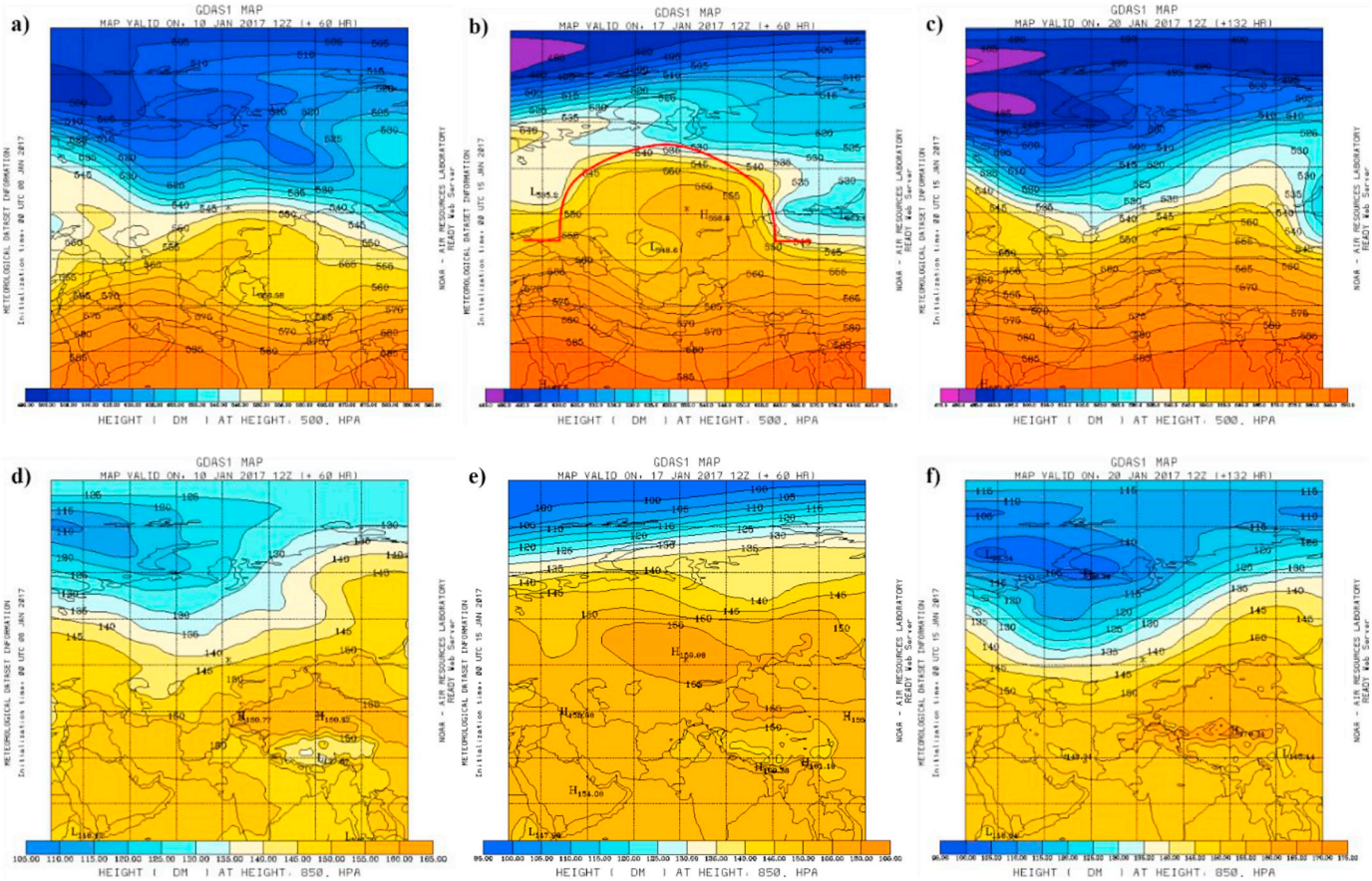

Fig. 7. The 500 hPa (5.5 km above sea level) and 850 hPa (1.5 km above sea level) geopotential height maps for the periods before (10 Jan 2017) (a and d), during (13 Jan 2017) (b and e) and after (20 Jan 2017) (c and f) the E2-W episode, respectively. The study area is in the center of the maps.

associated with all pollution levels.

A total of 21 long term episodic pollution periods, which are the members of top quantile pollution loads, more than a day period, typically lasting from several days to weeks in 2017, were identified. It was found that the majority of the episodes -especially winter smog episodes- have common characteristics associated with the mechanism of how pollution forms and evolves with anticyclone blockings. The common meteorological conditions for the heating period anticyclonic conditions were characterized by low wind speed, high ground-level pressures, and partly cloudy freezing weather conditions with the air temperature reaching −30 °C at night and − 20 °C in the daytime over several days. They typically lasted 3–9 days duration. They were most frequently observed in the middle of autumn and reached the highest peak during winter in 2017. There were also some summer smog episodes during stable weather conditions, which were, too, associated with the regional atmospheric circulations leading a thick photochemical smog in the atmosphere under the action of sunlight in the absence of wind when there is calm air with low humidity.

ECM types were defined using the Dzerdzeevskii et al. classification, and it was seen that this classification system explains at a decent level the pollution episodes and their relationships with the anticyclone blocking effects over the study area. The contribution of the ECM to pollution episodes was statistically investigated, and some of the ECMs found more stimulating to local pollution episodes. The most significant one is 13w type, since it is one of the most prevalent ECM types and contributed > 30% of all the events identified and 10% of the days in 2017. 13w type of circulation leads to the formation of cold weather in most parts of the country with Arctic invasions with downward air flows in an associated anticyclone, which press pollutants to the surface of the earth. When, mostly, it was experienced, the air of the study region shows typical characteristics with no precipitation, quiet, and still air, which intensifies the accumulation of pollutants with a thick smog cover over the city and, therefore, the concentration of the pollutants increase dramatically. Although some ECMs had low frequency, still they cause pollution episodes almost regularly when they appear (e.g., 5a, 5b, and 11a).

The results support that the regional climate conditions (e.g., wind, temperature, pressure, etc.) and ventilation characteristics of the atmospheric space of the city are essential factors for the accumulation of airborne pollutants in the surface layer of the atmosphere and their concentration remains at a higher level for longer terms, the episodes, particularly during anticyclone stagnation periodsIn total, 21 long-term pollution episodes, which are members of top-quantile pollution loads, were identified, typically lasting from several days to weeks in 2017. It was found that the majority of the episodes, especially winter smog episodes, have common characteristics associated with the mechanism of how pollution forms and evolves with anticyclone blockings. The common meteorological conditions for the anticyclonic conditions in the heating period were characterized by low wind speed, high ground-level pressures, and partly cloudy, freezing weather conditions with the air temperature reaching −30 °C at night and − 20 °C in the daytime over several days. They typically lasted 3–9 days. They were most frequently observed in the middle of autumn and reached the highest peak during winter 2017. There were also some summer smog episodes during stable weather conditions, which were also associated with the regional atmospheric circulations leading to a thick layer of photochemical smog in the atmosphere under the conditions of sunlight and low humidity in the absence of wind.

ECM types were defined using the Dzerdzeevskii et al. classification scheme, and it was observed that this classification system adequately

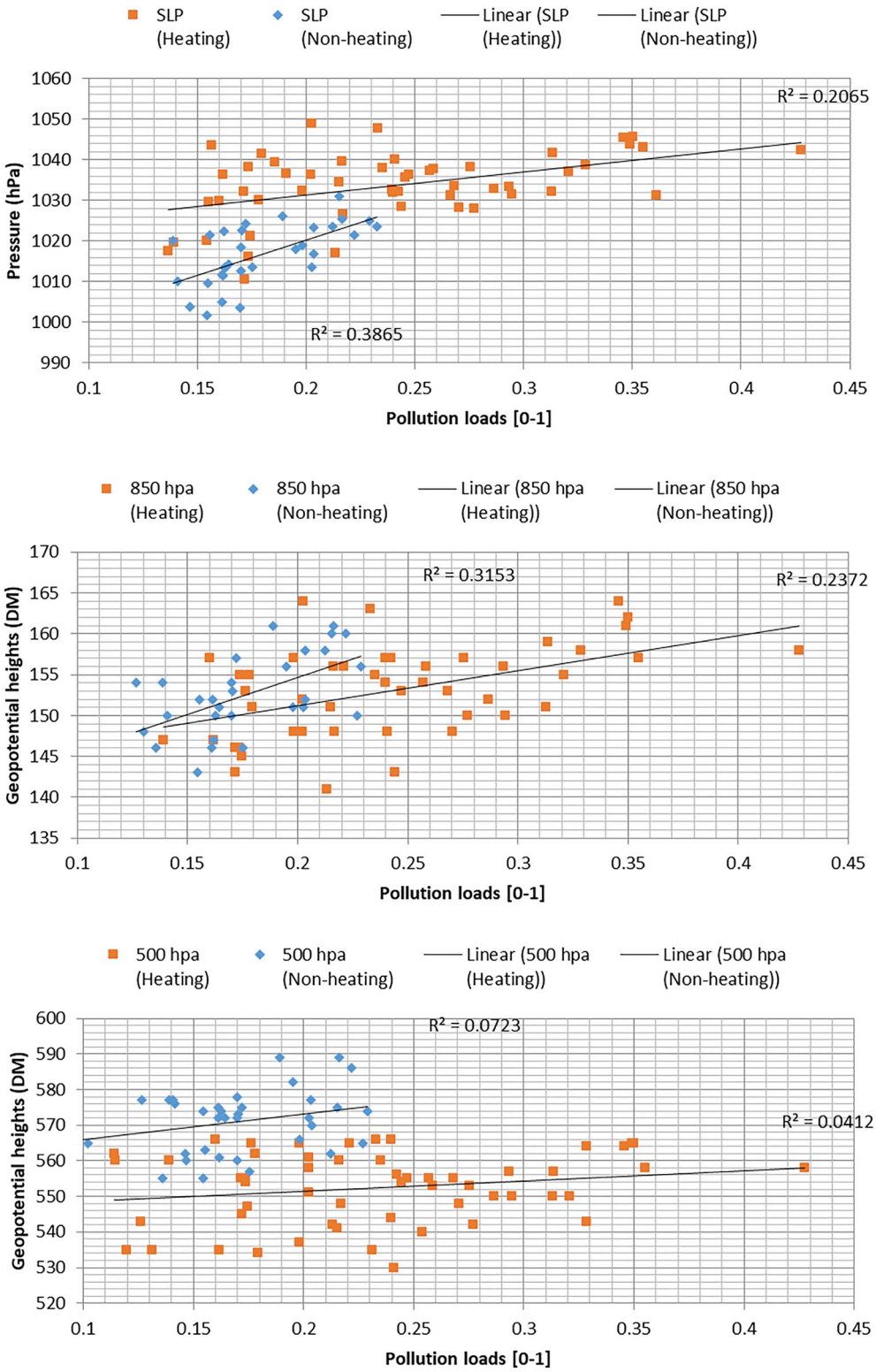

Fig. 8. Average surface level pressures (SLPs), the 850 hPa and 500 hPa geopotential heights vs. the pollution loads of the episodes.

explains the pollution episodes and their relationships with the anticyclone blocking effects over the study area. The contribution of the ECMs to pollution episodes was statistically investigated, and some of the ECMs were found to be more stimulating to local pollution episodes. The most significant one is the 13w type, since it is one of the most prevalent ECM type and contributed > 30% of all the events identified and 10% of the days in 2017. The 13w type of circulation leads to the formation of cold weather in most parts of the country with Arctic invasions with downward air flows in an associated anticyclone, which press pollutants to the surface of the earth. In general, the air in the study region shows typical characteristics of no precipitation and quiet, still air, which intensifies the accumulation of pollutants with thick smog cover over the city and, therefore, the concentration of the pollutants increases dramatically. Although some ECMs had a low

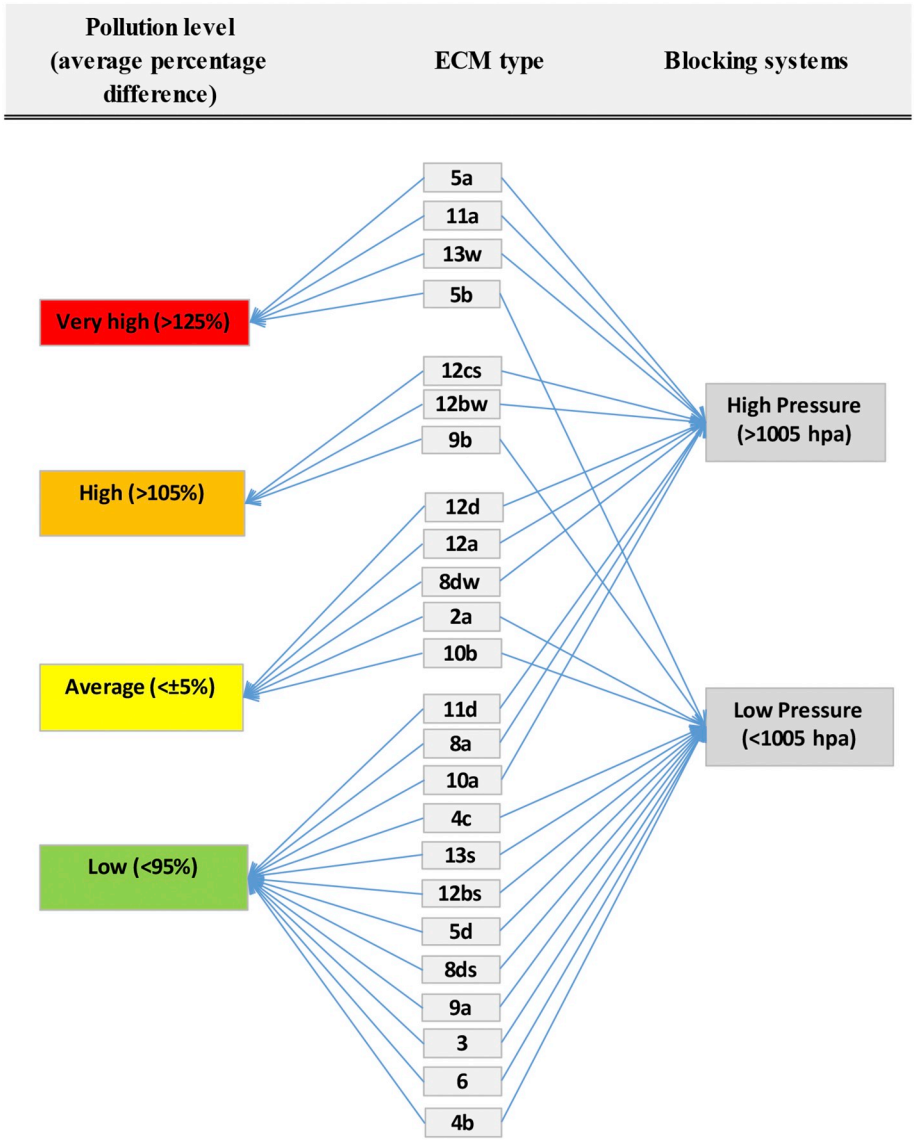

Fig. 9. A relationship diagram between the ECMs and their associated pressure systems and pollution levels.

frequency, they still cause pollution episodes almost regularly when they appear (e.g., 5a, 5b, and 11a).

The results support the conclusion that the regional climate conditions (e.g., wind, temperature, and pressure) and ventilation characteristics of the atmospheric space of the city are essential factors for the accumulation of airborne pollutants in the surface layer of the atmosphere, and their concentration remains at a higher level for a long time, particularly during anticyclone stagnation periods.

Declaration of Competing Interest

None.

Acknowledgments

The authors gratefully acknowledge the Program of Basic Research of the Institute of Geography, Russian Academy of Sciences, project no. 0148-2019-0009 for the provision of ECM related analyses; the RSE "KazHydroMet" organization for providing the national air quality monitoring (NAQM) data; and the NOAA Air Resources Laboratory (ARL) for the provision of the HYSPLIT transport model and READY website (http://www.ready.noaa.gov) used in this publication.

We thank anonymous reviewers for provided helpful comments on the earlier drafts of the manuscript.

Appendix A. Supplementary data

Supplementary data to this article can be found online at https://doi.org/10.1016/j.atmosres.2020.104858.

References

Amarsaikhan, D., Battsengel, V., Nergui, B., Ganzorig, M., Bolor, G., 2014. A Study on Air Pollution in Ulaanbaatar City, Mongolia. J. Geosci. Environ. Protect. 2, 123–128. https://doi.org/10.4236/gep.2014.22017.

Anil, I., Alagha, O., Karaca, F., 2017. Effects of transport patterns on chemical composition of sequential rain samples: trajectory clustering and principal component analysis approach. Air Qual. Atmos. Health 10 (10), 1193–1206. https://doi.org/10.1007/s11869-017-0504-x.

Antokhina, O.Y., Antokhin, P.N., Devyatova, E.V., Martynova, Y.V., 2018. 2004–2016 Wintertime atmospheric blocking events over western siberia and their effect on surface temperature anomalies. Atm. 9, 72. https://doi.org/10.3390/atmos9020072.

Bailey, A., Chase, T.N., Cassano, J.J., Noone, D., 2011. Changing Temperature Inversion Characteristics in the U.S. Southwest and Relationships to Large-Scale Atmospheric Circulation. J. Appl. Meteorol. Climatol. 50, 1307–1323. https://doi.org/10.1175/2011JAMC2584.1.

Barriopedro, D., García-Herrera, R., Lupo, A.R., Hernández, E., 2006. A climatology of

northern hemisphere blocking. J. Clim. 19 (6), 1042–1063. https://doi.org/10.1175/JCLI3678.1.
Brenčič, M., Kononova, N., Vreča, P., 2015. Relation between isotopic composition of precipitation and atmospheric circulation patterns. J. Hydrol. 529, 1422–1432. https://doi.org/10.1016/j.jhydrol.2015.08.040.
Chen, Y., Xie, S.D., 2014. Characteristics and formation mechanism of a heavy air pollution episode caused by biomass burning in Chengdu, Southwest China. Sci. Total Environ. 473-474, 507–517. https://doi.org/10.1016/j.scitotenv.2013.12.069.
Cheng, N., Li, Y., Cheng, B., Wang, X., Meng, F., Wang, Q., Qui, Q., 2018. Comparisons of two serious air pollution episodes in winter and summer in Beijing. J. Environ. Sc. 69, 141–154. https://doi.org/10.1016/j.jes.2017.10.002.
Draxler, R.R., Hess, G.D., 1998. An overview of the HYSPLIT_4 modeling system for trajectories, dispersion, and deposition. Aust. Meteorol. Mag. 47 (4), 295–308.
Dzerdzeevskii, B.L., 1962. Fluctuations of climate and of general circulation of the atmosphere in extra-tropical latitudes of the Northern Hemisphere and some problems of dynamic climatology. Tellus 14 (3), 328–336. https://doi.org/10.1111/j.2153-3490.1962.tb01345.x.
Dzerdzeevskii, B.L., Kurganskaja, V.M., Vitvitskaja, Z.M., 1946. Tipizacija cirkuljacionnyh mehanizmov v severnom polusharii i harakteristika sinopticheskih sezonov. [Classification of circulation mechanisms in Northern Hemisphere and characteristics of synoptic seasons: in Russian]. Trudy n.-i. uchrezhdenij Gl. upr. gidrometeorol. sluzhby pri Sovete Ministrov SSSR. Ser. 2 (21), 1–80.
Elansky, N., 2014. Air quality and CO emissions in the Moscow megacity. Urban Clim. 8, 42–56.
Fenech, S., Doherty, R.M., Heaviside, C., Macintyre, H.L., O'Connor, F.M., Vardoulakis, S., Neal, L., Agnew, P., 2019. Meteorological drivers and mortality associated with O3 and PM2.5 air pollution episodes in the UK in 2006. Atmos. Environ. 213, 699–710. https://doi.org/10.1016/j.atmosenv.2019.06.030.
Gangoiti, G., Alonso, L., Marino, N., Albizuri, A., Perez-Landa, G., Matabuena, M., Valdenebro, V., Maruri, M., García, J.A., Millán, M.M., 2002. Regional transport of pollutants over the Bay of Biscay: analysis of an ozone episode under a blocking anticyclone in west-Central Europe. Atmos. Environ. 36 (8), 1349–1361. https://doi.org/10.1016/S1352-2310(01)00536-2.
Gurjar, B.R., Butler, T.M., Lawrence, M.G., Lelieveld, J., 2008. Evaluation of emissions and air quality in megacities. Atmos. Environ. 42, 1593–1606.
Hassan, S.K., Khoder, M.I., 2017. Chemical characteristics of atmospheric PM2.5 loads during air pollution episodes in Giza, Egypt. Atmos. Environ. 150, 346–355. https://doi.org/10.1016/j.atmosenv.2016.11.026.
Hong, Q., Liu, C., Hu, Q., Xing, C., Tan, W., Liu, H., Huang, Y., Zhu, Y., Zhang, J., Geng, T., Liu, J., 2019. Evolution of the vertical structure of air pollutants during winter heavy pollution episodes: the role of regional transport and potential sources. Atmos. Res. 228, 206–222. https://doi.org/10.1016/j.atmosres.2019.05.016.
KazHydroMet, 2018. Ministry of Ecology, Geology and Natural Resources of the Republic of Kazakhstan, RSE "KazHydroMet". Newslett. State Environ. Republic Kazakhstan 1 (69), 13–15.
Kerimray, A., Bakdolotov, A., Sarbassov Inglezakis, V., Poulopoulos, S., 2018. Air pollution in Astana: analysis of recent trends and air quality monitoring system. Mater. Today 5 (11), 22749–22758. https://doi.org/10.1016/j.matpr.2018.07.086.
Kononova, N.K., 2009. Klassifikacija Cirkuljacionnyh Mehanizmov Severnogo Polusharija Po B.L. Dzerdzeevskomu [Classification of the Northern Hemisphere Circulation Mechanisms by BL Dzerdzeevskii: In Russian], Russian Academy of Sciences. Institute of Geography, Moscow, pp. 370.
Kononova, N.K., 2010. Long-term fluctuations of Northern Hemisphere atmospheric circulation according to Dzerdzeevskii's classification. Geogr. Environ. Sustain. 1 (3), 25–43. https://doi.org/10.24057/2071-9388-2010-3-1-25-43.
Kumar, K.R., Boiyo, R., Altayeva, M., Kang, N., 2018. A 13-year climatological study on the variations of aerosol and cloud properties over Kazakhstan from remotely sensed satellite observations. J. Atmospheric Sol.-Terr. Phys 179, 55–68. https://doi.org/10.1016/j.jastp.2018.06.014.
Lee, H.S., Jhun, J.G., 2006. Two types of the Asian continental blocking and their relation to the East Asian monsoon during the boreal winter. Geophys. Res. Lett. 33, 1–5. https://doi.org/10.1029/2006GL027948.
Lejenas, H., Holmén, K., 1996. Characteristics of the large-scale circulation during episodes with high and low concentrations of carbon dioxide and air pollutants at an arctic monitoring site in winter. Atmos. Environ. 30 (17), 3045–3057. https://doi.org/10.1016/1352-2310(96)00004-0.
Liu, N., Zhou, S., Liu, C., Guo, J., 2019. Synoptic circulation pattern and boundary layer structure associated with PM2.5 during wintertime haze pollution episodes in Shanghai. Atmos. Res. 228, 186–195. https://doi.org/10.1016/j.atmosres.2019.06.001.
Lupo, A.R., Oglesby, R.J., Mokhov, I.I., 1997. Climatological features of blocking anticyclones: a study of Northern Hemisphere CCM1 model blocking events in present-day and double CO2 concentration atmospheres. Clim. Dyn. 13 (3), 181–195. https://doi.org/10.1007/s003820050159.
Malek, E., Davis, T., Martin, R.S., Silva, P.J., 2006. Meteorological and environmental aspects of one of the worst national air pollution episodes (January, 2004) in Logan, Cache Valley, Utah, USA. Atmos. Res. 79, 108–122. https://doi.org/10.1016/j.atmosres.2005.05.003.
Michaelides, S., Paronis, D., Retalis, A., Tymvios, F., 2017. Monitoring and forecasting air pollution levels by exploiting satellite, ground-based, and synoptic data, elaborated with regression models. Adv. Meteorol. 2954010, 17. https://doi.org/10.1155/2017/2954010.
Mokhov, I.I., Timazhev, A.V., Lupo, A.R., 2014. Changes in atmospheric blocking characteristics within Euro-Atlantic region and Northern Hemisphere as a whole in the 21st century from model simulations using RCP anthropogenic scenarios. Glob. Planet. Chang. 122, 265–270. https://doi.org/10.1016/j.gloplacha.2014.09.004.
Molepo, K.M., Abiodun, B.J., Magoba, R.N., 2019. The transport of PM10 over Cape Town during high pollution episodes. Atmos. Environ. 213, 116–132. https://doi.org/10.1016/j.atmosenv.2019.05.041.
Monteiro, A., Gouveia, S., Scotto, M., Sorte, S., Gama, C., Gianelle, V.L., Colombi, C., Alves, C., 2018. Investigating PM10 episodes using levoglucosan as tracer. Air Qual. Atmos. Health 11 (1), 61–68. https://doi.org/10.1007/s11869-017-0521-9.
Nascimento, E.L., Ambrizzi, T., 2002. The influence of atmospheric blocking on the rossby wave propagation in Southern Hemisphere winter flows. J. Meteorol. Soc. JPN Ser. II. 80 (2), 139–159. https://doi.org/10.2151/jmsj.80.139.
Nishanbaeva, L., 2015. Report on Air and Water Quality Indicators in Kyrgyzstan. MONECA Component of the FLERMONECA Project. Available online (in Russian). http://naturalresources-centralasia.org/flermoneca/assets/files/Report%20air%20quality-KG.pdf (last visited on 23/10/2019).
Pfahl, S., Schwierz, C., Croci-Maspoli, M., Grams, C.M., Wernli, H., 2015. Importance of latent heat release in ascending air streams for atmospheric blocking. Nat. Geosci. 8, 610–614. https://doi.org/10.1038/NGEO2487.
Rex, D.F., 1950a. Blocking action in the middle troposphere and its effect upon regional climate. Part I: an aerological study of blocking action. Tellus 2, 196–211. https://doi.org/10.1111/j.2153-3490.1950.tb00331.x.
Rex, D.F., 1950b. Blocking action in the middle troposphere and its effect upon regional climate. Part II: the climatology of blocking action. Tellus 2, 275–301. https://doi.org/10.1111/j.2153-3490.1950.tb00339.x.
Rolph, G., Stein, A., Stunder, B., 2017. Real-time environmental applications and Display sYstem: READY. Environ. Model. Softw. 95, 210–228. https://doi.org/10.1016/j.envsoft.2017.06.025.
Rupakheti, D., Kang, S., Bilal, M., Gong, J., Xia, X., Cong, Z., 2019. Aerosol optical depth climatology over Central Asian countries based on Aqua-MODIS Collection 6.1 data: Aerosol variations and sources. Atmos. Environ. 207, 205–214. https://doi.org/10.1016/j.atmosenv.2019.03.020.
Shin, S.K., Lee, K.H., Park, S.S., Wong, M.S., 2017. Synergetic analysis of springtime air pollution episodes over Gwangju, Korea. J. Environ. Sc. 57, 270–283. https://doi.org/10.1016/j.jes.2017.02.002.
Sun, J., Gong, J., Zhou, J., Lui, J., Liang, J., 2019. Analysis of PM2.5 pollution episodes in Beijing from 2014 to 2017: Classification, interannual variations and associations with meteorological features. Atmos. Environ. 123, 384–394. https://doi.org/10.1016/j.atmosenv.2019.06.015.
Toro, A.R., Kvakic, M., Klaic, Z.B., 2019. Exploring atmospheric stagnation during a severe particulate matter air pollution episode over complex terrain in Santiago, Chile. Environ. Pollut. 244, 705–714. https://doi.org/10.1016/j.envpol.2018.10.067.
Trigo, R.M., Trigo, I.F., Dacamara, C.C., Osborn, T.J., 2004. Winter blocking episodes in the European-Atlantic sector: climate impacts and associated physical mechanisms in the NCEP reanalysis. Clim. Dyn. 23, 17–28. https://doi.org/10.1007/s00382-004-0410-4.
Tyrlis, E., Hoskins, J., 2007. Aspects of a northern hemisphere atmospheric blocking climatology. J. Atmos. Sci. 65 (5), 1638–1652. https://doi.org/10.1175/2007JAS2337.1.
Vu, T.V., Shi, Z., Cheng, J., et al., 2019. Assessing the impact of clean air action on air quality trends in Beijing using a machine learning technique, Atmos. Chem. Phys. 19, 11303–11314.
Wang, Y.Q., Zhang, X.Y., Draxler, R.R., 2009. TrajStat: GIS-based software that uses various trajectory statistical analysis methods to identify potential sources from long-term air pollution measurement data. Environ. Model. Softw. 24, 938–939. https://doi.org/10.1016/j.envsoft.2009.01.004.
Wang, Y., Yao, L., Wang, L., Liu, Z., Ji, D., Tang, G., Zhang, J., Sun, Y., Hu, B., Xin, J., 2014. Mechanism for the formation of the January 2013 heavy haze pollution episode over central and eastern China. Sci. China Earth Sci. 57 (1), 14–25. https://doi.org/10.1007/s11430-013-4773-4.
Zhao, D., Xin, J., Gong, C., Quan, J., Liu, G., Zhao, W., Wang, Y., Liu, Z., Song, T., 2019. The formation mechanism of air pollution episodes in Beijing city: Insights into the measured feedback between aerosol radiative forcing and the atmospheric boundary layer stability. Sci. Total Environ. 692, 371–381. https://doi.org/10.1016/j.scitotenv.2019.07.255.
Zhou, C., Wei, G., Xiang, J., Zhang, K., Li, C., Zhang, J., 2018. Effects of synoptic circulation patterns on air quality in Nanjing and its surrounding areas during 2013–2015. Atmos. Pollut. Res. 9, 723–734. https://doi.org/10.1016/j.apr.2018.01.015.